The correlation between the mixed-mode oligo-cyclic loading induced mechanical and microstructure changes in HDPE

Hang Guo, R.G. Rinaldi, Sourour Tayakout, Morgane Broudin, Olivier Lame

▶ **To cite this version:**

Hang Guo, R.G. Rinaldi, Sourour Tayakout, Morgane Broudin, Olivier Lame. The correlation between the mixed-mode oligo-cyclic loading induced mechanical and microstructure changes in HDPE. Polymer, 2021, 224, 10.1016/j.polymer.2021.123706 . hal-03483679

HAL Id: hal-03483679
https://hal.science/hal-03483679

Submitted on 24 Apr 2023

HAL is a multi-disciplinary open access archive for the deposit and dissemination of scientific research documents, whether they are published or not. The documents may come from teaching and research institutions in France or abroad, or from public or private research centers.

L'archive ouverte pluridisciplinaire **HAL**, est destinée au dépôt et à la diffusion de documents scientifiques de niveau recherche, publiés ou non, émanant des établissements d'enseignement et de recherche français ou étrangers, des laboratoires publics ou privés.

Distributed under a Creative Commons Attribution - NonCommercial 4.0 International License

Version of Record: https://www.sciencedirect.com/science/article/pii/S0032386121003293
Manuscript_1206735aac5f295d0a0f4eaadeb39b06

The correlation between the mixed-mode oligo-cyclic loading induced mechanical and microstructure changes in HDPE

*Hang GUO[1], Renaud G. RINALDI[1], Sourour TAYAKOUT[2], Morgane BROUDIN[3], Olivier LAME[1]**

[1)] Université de Lyon, CNRS, INSA-Lyon, MATEIS, UMR5510, 69621, Villeurbanne, France

[2)] EDF-DIPNN-Direction Technique, 19 rue Pierre Bourdeix, F-69007, LYON, France

[3)] EDF-R&D Lab Les Renardières, Avenue des Renardières-Ecuelles, F-77250, Moret-Loing-et-Orvanne, France

ABSTRACT

Two grades of HDPE (one is for PE-100 pipeline application and one is for blow molding) were processed to vary their crystallinity and molecular topology in order to investigate and understand the microstructural origin of the seismic performance of HDPE materials. For a given grade, the quenched sample exhibits a lower crystallinity, thinner crystallites, and a higher density of entanglement/tie molecules compared to the isothermal one. The HDPE samples are submitted to mixed-mode, oligo (plastic)-cyclic tensile deformation (that simulates the seism) with the applied maximum strain below or at the onset of necking propagation. The changes of numerous macroscopic mechanical metrics with increasing cycles were monitored (e.g. stress at maximum strain, residual strain at zero stress, secant modulus, and hysteresis loop area). These mechanical changes not only depend on the maximum imposed cyclic strain, but also the microstructure of HDPE. A physical scenario is proposed to describe the microstructural changes during the cyclic deformation and explicate the macro-micro correlations. Moreover, the post-cyclic tensile (reloading) curve can return to the original one rapidly for each sample, this phenomenon indicates the neglecting effect of the following cycles on the further loading path. It is also found that the material designed for the PE-100 pipeline shows limited variation between the initial and post-cyclic tensile toughness, indicating that the pre-loaded materials require nearly the same energy to rupture as the pristine ones. This is evidence that the material for PE-100 pipeline has a good resistance against the damage induced by seismic events.

© 2021 published by Elsevier. This manuscript is made available under the CC BY NC user license
https://creativecommons.org/licenses/by-nc/4.0/

KEYWORDS: HDPE, oligo-cyclic tensile loading conditions, macro-micro correlations, tensile toughness

INTRODUCTION

High-density polyethylene (HDPE) is widely used in industrial pipeline applications. PE 80 and PE 100 refer to common grades applied for gas and/or water pipelines. Among other benefits, pipelines made of HDPE exhibit a great resistance against seismic events[1,2], which are normally modeled by repeated loading-unloading cycles beyond the elastic limit (also defined as low cycle fatigue tests or oligo-cyclic tests)[3,4]. Therefore, it is valuable to carry out the investigations on the overall mechanical performances along with the deformation mechanisms and the damage evaluation in HDPE under (oligo-) cyclic loading conditions.

At the microscale, HDPE is a well-known semi-crystalline polymer consisting of crystalline and amorphous phases, connected by tie molecules/entanglement. The microstructural changes occurring throughout the small strain viscoelastic to the large strain plastic regimes during monotonic tensile tests in HDPE have been widely discussed for a long time[5–11]. The correlations between several mechanical indicators obtained from the stress-strain tensile profiles and the microstructure of HDPE are well established. In the elastic regime, the storage/elastic modulus is governed by the fraction of crystalline phase, apparent amorphous modulus, and percolation of the crystalline structure[9,12]. At the onset of plasticity, the quasi-linear relation between the threshold stress and crystallinity is associated with the dislocation model (thickness of crystalline lamellae) and the concept of stress transmitters (STs)[10,11]. It worth noting that insights regarding the amorphous chains topology or density of stress transmitters (ST density) were also obtained by mechanical measurements such as the neck width[11], natural draw ratio, and hardening[7,11,13]. The STs include the tie molecules and the entangled loops/chains, they are capable of transmitting the stress and they are also believed to play a crucial role in long-term properties such as creep, fatigue behaviors[14–17] as well as the crack propagation and cavitation [16,18–20].

In the literature, procedures can vary to perform (oligo-) cyclic tensile tests: for so-called stress-controlled[21–27] or strain-controlled modes[28,29], the cyclic paths are conducted between two prescribed forces (stresses) or displacements (strains) respectively. Besides these two modes, mixed-mode conditions can also be used[30–33], for which the sample is repeatedly

stretched to a prescribed maximum strain and then retracted to zero force. During the cyclic tests, the mechanical indicators (e.g. stress, strain, modulus, hysteresis area) are seen to evolve with the increasing number of cycles suggesting microstructural modifications. The change of the elastic modulus has been attributed to two competing mechanisms. On the one hand, the modulus decrease is related to the cavitation (or micro-voids) and/or fragmentation of crystalline lamellae[24,29,34,35]. Generally, this mechanical loss is recognized as a macroscopic symbol of material damage[29,35]. On the other hand, the chain orientation might lead to an increase of the modulus along with the tensile deformation, also defined as "cyclic strengthening" as suggested by Drozdov[29]. Additionally, the density of dissipated energy of each stress-strain cycle, calculated as the hysteresis area, is ascribed to the generated heat by the plastic deformation and viscous loss mechanisms[36]. This parameter is related to the failure mode and lifetime of polymers[26,36,37].

Moreover, the accumulation of residual strain (by stress-controlled or mixed modes) and the stress softening (by strain-controlled or mixed modes) are also relevant features to probe the microstructural changes[21,23,25,29,31–33]. In particular, during mixed-mode cyclic tests, the semi-crystalline polymers display both stress softening at maximum strain and the accumulation of residual strain at zero stress with increasing cycles[31,32]. These two phenomena are largely considered as the macroscopic features of the *Mullins-like* effect, thus differing from the classically so-called *Mullins* effect enounced in the filled and crystallizing rubbers[38–40]. In detail, the first hysteresis loop is significantly different from the following ones, which is recognized as a primary property of the *Mullins-like* effect[32,41]. Although the mechanisms are complex and controversial, the network alteration theory has been successfully applied to explain this phenomenon. Makki et *al.*[32] described the microstructural changes of the *Mullins-like* effect in PE basing on a framework proposed for styrene-butadiene rubber[42]. In their work, the authors assign the difference in mechanical behaviors between the first cycle and the following ones to the rearrangement of the network. During the following cycles (after the first one), the additional rupture of chains reaching their limit extensibility is associated with the stress softening behavior. Moreover, a new equilibrium state at zero stress leads to an increase in the residual strain. Another striking manifestation of the *Mullins* phenomenon is that the post-cyclic reloading response for strain greater than the one already endured by the material coincides with the pristine response [38–40]. This phenomenon has been observed in polypropylene[31], with

the maximum applied strain in the vicinity of the yield point. However, few studies discuss the post-cyclic behavior in PE, especially the properties related to the final rupture such as tensile toughness.

In this work, investigations of the *Mullins-like* stress softening/accumulation of residual strain in HDPE samples with different pristine microstructures and molecular topologies are carried out. Noticeably, mixed-mode oligo-cyclic tests with maximum strains preventing pronounced necking (below or at the onset of necking propagation phase) are performed. This strain range ascertains that the lamellar or spherulitic structure globally remains and the fibrillary structure[7,12,43,44] induced by large deformation is not completely formed. The relative changes of the secant modulus and hysteresis loop areas are also computed. A physical scenario is proposed to interpret the correlation between the mechanical changes and the pristine microstructure of the PE samples. Moreover, the post-cyclic mechanical behaviors are also discussed.

EXPERIMENTAL SECTION

Materials

Two types of HDPE denoted PE-A and PE-B, are studied. PE-A refers to a blow molding grade and PE-B is a grade for the commercial PE-100 widely used in piping application. The molar masses were characterized and provided by the supplier INEOS (Brussels, Belgium) (see **Table 1**). The PE pellets were pressed into about 0.5 mm plates at 180°C in an aluminum-alloy mold. Once molded, quenching and isothermal thermal treatments were performed in order to vary the pristine microstructures of the two materials. The "quenched samples" were shaped in cold water whereas the "isothermal samples" were shaped in the oil bath for about 17h at a temperature T_{iso} around the crystallizing temperature, yet preventing the secondary crystallization[45,46].

Table 1: Initial molecular characteristics and T_{iso} of the polyethylene pellets

Materials	M_n (g/mol)	M_w (g/mol)	M_z (g/mol)	T_{iso} (°C)
PE-A	7500	202200	1478900	121.5
PE-B	6700	270800	1589400	118

M_n, M_w and M_z are the number-average molar mass, the weight-average molar mass and z-average molar mass.

Differential Scanning Calorimetry (DSC) tests

6 to 10 mg samples were taken from the HDPE plates and heated up to 150°C at 10°C/min with a DSC 7 PerkinElmer machine under nitrogen flow. The following equation (1) was used to estimate the material's crystallinity (X_c):

$$X_c = \frac{\Delta H_f}{\Delta H_f^0} \quad (1)$$

Where ΔH_f is the melting enthalpy calculated as the area under the DSC melting peak and ΔH_f^0 is the melting enthalpy of polyethylene of 100% crystallinity (290 J/g[47]). The overall density ρ could thus be estimated as follow:

$$\frac{1}{\rho} = \frac{X_c}{\rho_c} + \frac{1-X_c}{\rho_a} \quad (2)$$

Where ρ_c is the crystalline phase density (1.003 g/cm^3), ρ_a is the amorphous phase density (0.850 g/cm^3) [48]. X_c and ρ were also used for calculating the thickness of crystalline lamellae as shown in the next subsection.

SAXS (Small-angle X-ray scattering) characterizations

The small-angle X-ray scattering experiments were performed on the SWING beamline of the French SOLEIL synchrotron with the X-ray wavelength of 0.103 nm. The sample-detector distance was 2003 mm so that the scattering vector q ranged between 0.036 and 0.52 $Å^{-1}$. The determination of the long period (L_p), the thicknesses of crystalline lamellae (L_c), and the amorphous layers (L_a) were obtained according to equations (3), (4) and (5).

$$L_p = \frac{2\pi}{q_{max}} \quad (3)$$

$$L_c = L_p \frac{\rho}{\rho_c} X_c \quad (4)$$

$$L_a = L_p - L_c \quad (5)$$

It worth noting that the scattering wave vector q_{max} corresponds to the maximum *Lorentz-corrected* scattering intensity. These nano-dimensions could be used for the estimation of the ST density by Brown's model[7,13,49,50] and for building the macro-micro correlations.

Mechanical tests: Uniaxial tensile, mixed-mode oligo-cyclic tensile and multi-step tests

Mechanical tests (uniaxial tensile, mixed-mode oligo-cyclic tensile, and multi-step tests) were performed on dumbbell-shaped samples of 8 mm gauge length, 4 mm width, and about 0.5 mm

thickness punched out of the polymer sheets at room temperature. The tests were conducted using an MTS 1/ME machine equipped with a 100N load cell at a nominal strain rate $\dot{\varepsilon} = 3 \times 10^{-3} s^{-1}$.

Uniaxial tensile tests were conducted till failure to guide the selection of the oligo-cyclic strain ε_{OC} (the maximum imposed strain in each cycle). These tests also allow characterizing the mechanical properties such as the neck width[11] and initial tensile toughness defined as the area under the stress-strain profile until failure. 100 mixed-mode cycles with ε_{OC} = 0.08/0.16/0.24/0.5 were performed. In multi-steps tests, the samples were initially subjected to 10 mixed oligo-cycles with the same ε_{OC} = 0.08/0.16/0.24/0.5 and then immediately stretched up to failure, special attention is drawn to the post-cyclic behavior in each sample.

RESULTS AND DISCUSSION

Pristine microstructural characteristics

The microstructural properties (crystallinity X_c, long period L_p, thickness of crystallites L_c, and thickness of amorphous layers L_a) of the PE materials are listed in **Table 2**. It worth noting that L_c and L_a are precisely obtained according to the results of SAXS, the deviation is too small to present. As for crystallinity measurement, the deviation is $\pm 1\%$. The density of STs has been approximated by both the statistic approach (Brown's model)[7,13,49,50] and the neck width[11] (with deviation ± 0.05) measured from the nominal uniaxial tensile stress-strain curves reported in **Figure 1**. The PE having enhanced ST density tends to exhibit a more diffuse neck indicating a more homogenous deformation[8,11]. The results obtained by these two methods are consistent with each other. For a given grade (PE-A or PE-B), the isothermal sample has a relatively higher crystallinity, thicker crystallites, and lower ST density[5,11,51] thanks to its slower crystallization process[45] compared to the quenched sample.

Table 2. Crystallinity X_c, long period L_p, thickness of crystallites L_c and amorphous layers L_a, ST density estimated by Brown's model and neck width of PE plates subjected to different thermal treatments.

Methods		DSC	SAXS			Brown's model	Neck width
Material characteristics		X_c (%)	L_p (nm)	L_c (nm)	L_a (nm)	ST density	
PE-A	Quenched	62	22	13	9	0.22	0.55
	Isothermal	73	35	24	11	0.07	0.27
PE-B	Quenched	57	20	11	9	0.27	0.65
	Isothermal	64	33	20	13	0.14	0.32

Mixed-mode oligo-cyclic tensile behaviors

Figure 1 superimposes the nominal uniaxial (up to a nominal strain $\varepsilon = 1$) and the oligo-cyclic tensile stress-strain profiles (maximum applied strain $\varepsilon_{OC} = 0.08$, 0.16, 0.24 and 0.5) of all four PE samples. The 2nd and 100th cycles are highlighted for better reading of the overall change of the mechanical loops. Throughout the mixed-mode oligo-cyclic tests, the stress at maximum strain, the residual strain at zero stress, the tangent modulus and the hysteresis response are seen to evolve and progressively saturate as the cycle number increases.

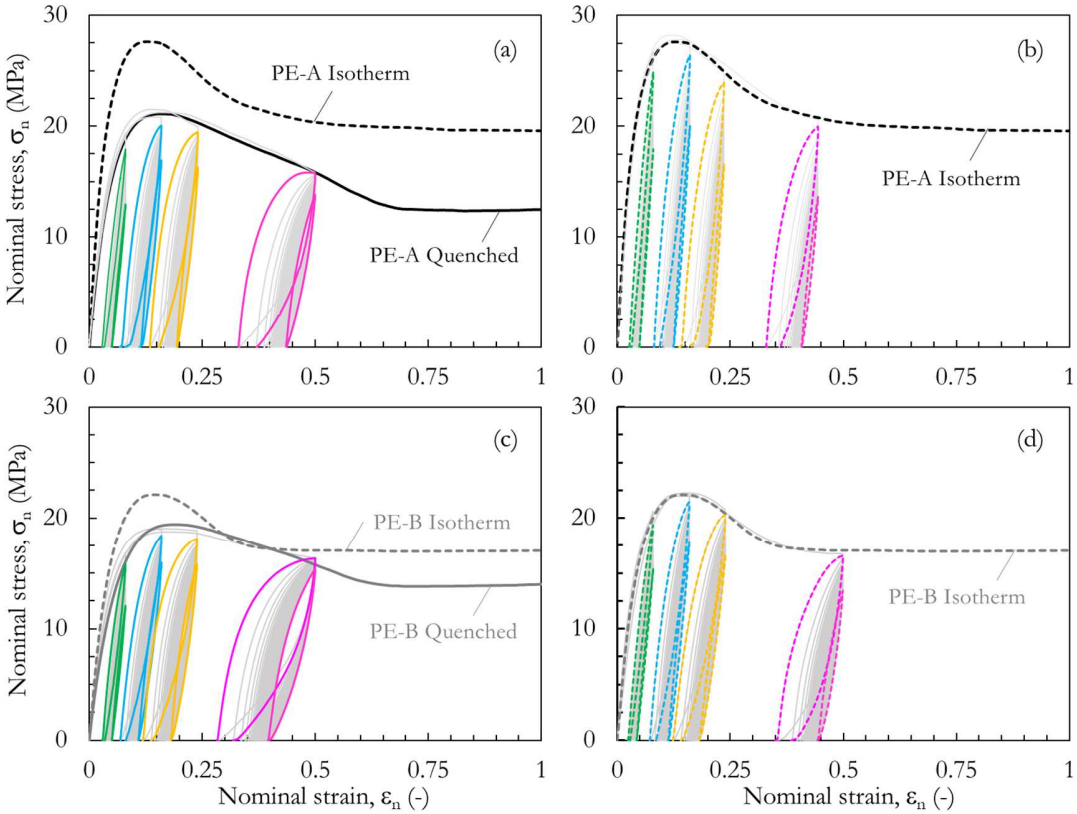

Figure 1: Nominal uniaxial and oligo-cyclic tensile stress-strain profiles.

(ε_{OC} = 0.08, 0.16, 0.24 and 0.5).

In order to quantify the mechanical alterations during the oligo-cyclic tests and tend to express their dependencies on the pristine sample microstructure and/or ε_{OC} values, several mechanical indicators are monitored. They are illustrated in **Figure 2** and defined as follow:

- σ_{oc}^{i}: The nominal stress corresponding to the maximum-strain state at i^{th} cycle ($1 \leq i \leq 100$).
- $\Delta\sigma^{i-1}$: The magnitude of stress softening between 1^{st} and i^{th} cycle ($2 \leq i \leq 100$).
- ε_{res}^{i}: The residual strain at zero-stress state at i^{th} cycle ($1 \leq i \leq 100$).
- $\varepsilon_{res}^{2-100}$: The residual strain at zero-stress state induced by the following cycles (from 2^{nd} to 100^{th}).
- ε_{OC}: The applied maximum strain in oligo-cyclic tests.
- W_{d}^{i}: The hysteresis energy corresponding to the dissipated energy per unit volume at i^{th} cycle ($1 \leq i \leq 100$).

- E^i: Secant modulus of i^{th} cycle determined as $E^i = \frac{\sigma_{oc}^i}{\varepsilon_1^i}$, where $\varepsilon_1^i = \varepsilon_{OC}^i - \varepsilon_{res}^{i-1}$ $(2 \leq i \leq 100)$.
- E_1^i: Comparative modulus measured in the first cycle within the same span of strain ε_1^i as $E^i(2 \leq i \leq 100)$. It is used for evaluating the relative change of modulus from the 1st to the i^{th} cycle. The detail of the calculation will be introduced in the following section *Change of modulus*.

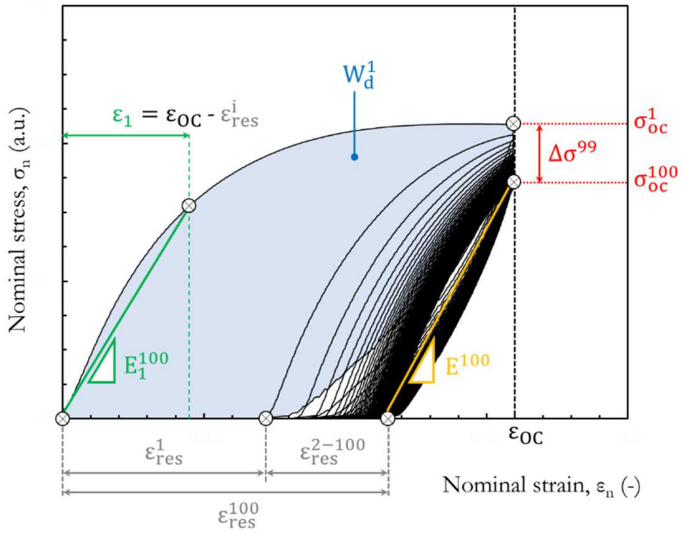

Figure 2: Oligo-cyclic curve with the description of the evaluated mechanical changes.

Mechanical alterations and associated mechanisms

Stress softening

As shown in **Figure 3**, the stress-softening magnitude ($\Delta\sigma$) decreases as ε_{OC} increases for all the four samples whatever the cycle number. The negative correlation between the total stress softening magnitudes $\Delta\sigma^{99}$ and ε_{OC} is further displayed, in **Figure 4a**.

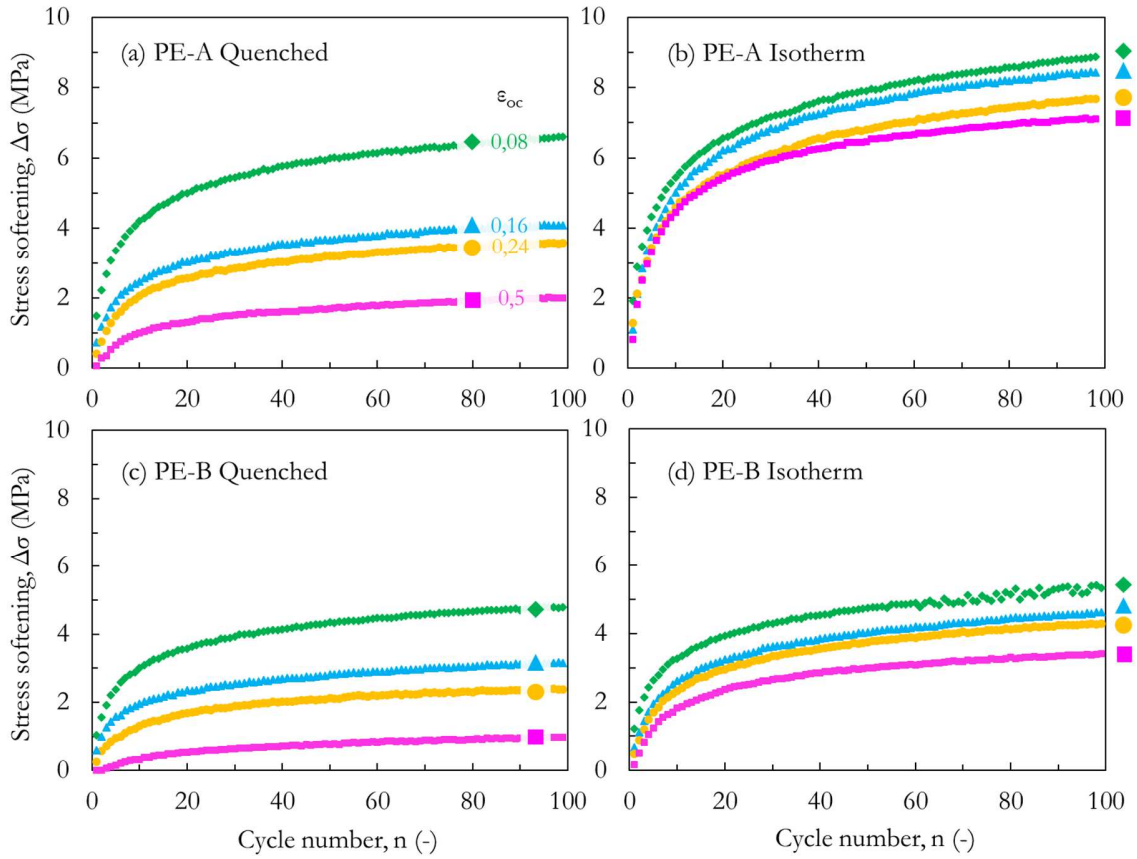

Figure 3: Stress-softening magnitude in different samples as a function of cycle number: (a) PE-A Quenched; (b) PE-A Isothermal; (c) PE-B Quenched and (d) PE-B Isothermal

For a given grade, it worth noting that more pronounced stress softening is observed in the isothermal sample when ε_{OC} is identical. Moreover, an indicator $\Delta\sigma^*$ determined by **equation (6)** is evoked for evaluating the improvement of the stress-softening resistance with increasing ε_{OC} in each sample (from $\varepsilon_{OC} = 0.08$ to $\varepsilon_{OC} = 0.5$). In particular, when $\varepsilon_{OC} = 0.08$, $\Delta\sigma^*$ is set as zero.

$$\Delta\sigma^*(\varepsilon_{OC}) = \frac{\Delta\sigma^{99}(0.08) - \Delta\sigma^{99}(\varepsilon_{OC})}{\Delta\sigma^{99}(0.08)} \quad (6)$$

As shown in **Figure 4b,** it has been found that $\Delta\sigma^*$ also depends on the PE initial microstructure. A more significant increase of $\Delta\sigma^*$ is observed in the sample with lower crystallinity and higher ST density.

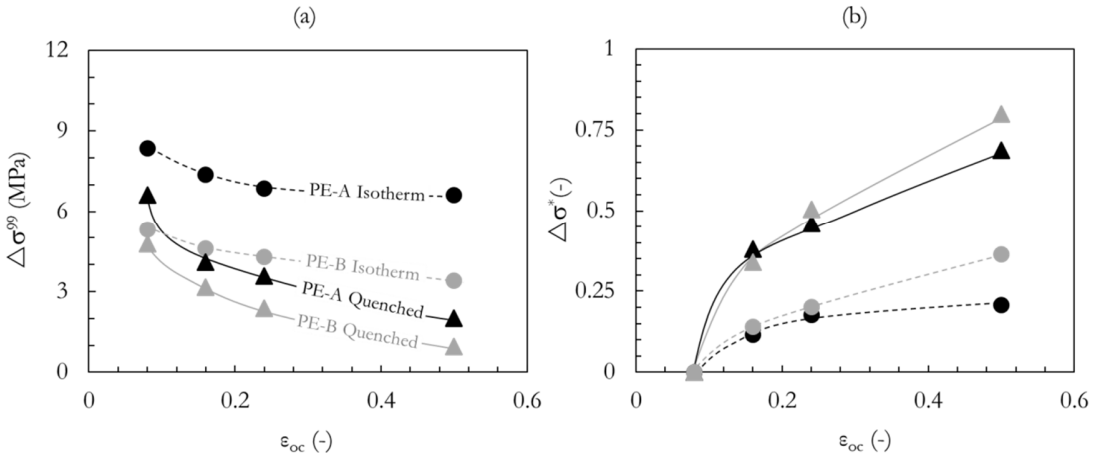

Figure 4: a) Total stress-softening magnitudes between 1st and 100th loading; b) Relative decrease of stress softening as a function of ε_{OC} in different samples

Various authors have attempted to figure out the physical interpretation of the cyclic stress-softening phenomenon in semi-crystalline polymers. However, the mechanisms remain disputable. Firstly, the rupture of short chains reaching their limit of extensibility, along with the disentanglement and breakdown of chains being stuck between two entanglement/crystallites are raised[32,42]. These mechanisms occurring in the amorphous phase could also potentially induce cavitation[35]. Furthermore, when a semi-crystalline polymer is deformed beyond yielding, the fragmentation of crystallites can also be considered as an origin of the macroscopic material softening[35]. This phenomenon could also be related to the elimination of the crystalline percolation.

The aforementioned dependencies of stress softening on ε_{OC} and PE microstructure can be explicated as follow: i) the stress-softening-related microstructure changes are mainly induced by the first cycle. And the higher ε_{OC}, the more important these structural changes. As these phenomena could induce the softening, they are thus globally named as "structural deteriorations" in the following sections. As the ε_{OC} increases, the microstructure after the 1st cycle tends to become an "extreme state" where the crystalline percolation is all eliminated and the remained STs are difficult to be disentangled/ruptured by the following cycles, the progressive stress-softening is thus more limited. ii) It has another compensating mechanism being stronger with increasing ε_{OC}. Also, its enhancement with increasing ε_{OC} should be more pronounced in the samples with lower crystallinity but higher ST density due to the lower value

of stress softening. As mentioned in the introduction, under uniaxial tensile loading, the stress transmitters can be highly stretched, oriented along the loading direction, and induce recrystallization[52]. This phenomenon is related to the strengthening effect and should compensate for the stress softening[29,53]. Also, it is reasonable that this compensating phenomenon is more important in the samples with more STs [10,11] that promote their stretching and strain-induced recrystallization.

Residual strain accumulation

The residual strain (or inelastic strain) ε_{res} in semi-crystalline polymers can be divided into two parts, one being associated with the plastic deformation whereas the other one is due to the viscous effect of the amorphous phase that can be recovered after relaxation[31,40,41]. The residual strain accumulation-saturation behavior in each sample is displayed in **Figure 5.** The first-cycle-induced residual strain is the most important one.

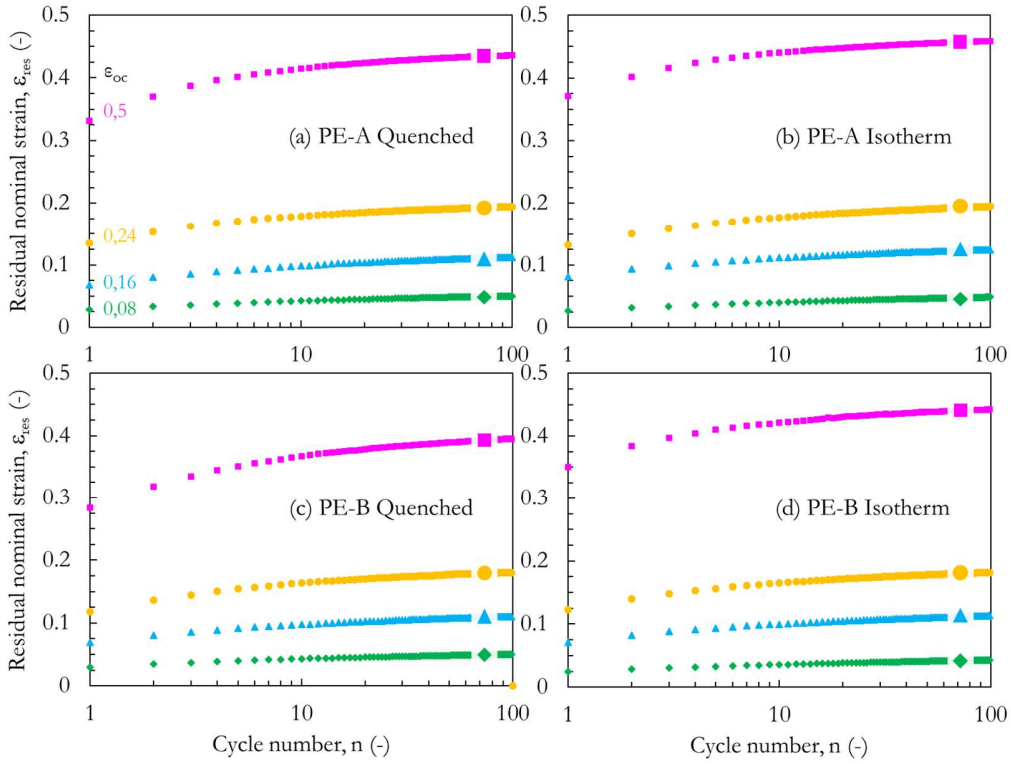

Figure 5: Residual strain in different samples as a function of cycle number: (a) PE-A Quenched; (b) PE-A Isothermal; (c) PE-B Quenched and (d) PE-B Isothermal

Moreover, ε_{res}^{1} and $\varepsilon_{res}^{2-100}$ as a function of ε_{OC} are shown in **Figure 6a** and **6b** respectively. For all samples, with increasing ε_{OC}, the inelastic strains induced by the first and the remaining cycles are both seen to increase. For ε_{OC} = 0.08, 0.16, and 0.24, the difference in residual strains between the four materials is not clearly measurable. However, when ε_{OC} = 0.5, the ε_{res}^{1} is larger in the samples with higher crystallinity, whereas the tendency is the opposite for $\varepsilon_{res}^{2-100}$.

As a physical interpretation, when the imposed strain in the first cycle is high enough (i.e. ε_{OC} = 0.5), The percolation of the crystalline network is most likely ruptured in numerous locations during the first cycle, and the majority of the residual strain can be considered as the irreversible/plastic one. The plasticity is thus stronger in the sample with higher crystallinity. However, the residual strain induced by the following cycles could be mainly attributed to the deformation in the amorphous phase. Therefore, the sample with lower crystallinity should have a macromolecular network more "inelastically" deformable due to the larger quantity of STs. However, in the lower strain range (ε_{OC} = 0.08, 0.16 and 0.24), the crystalline network is not completely broken by the first loading, the following cycles may continually and slightly induce the residual strains in both the crystalline and amorphous phases, thus, the magnitudes of ε_{res}^{1} and $\varepsilon_{res}^{2-100}$ are not clearly differed.

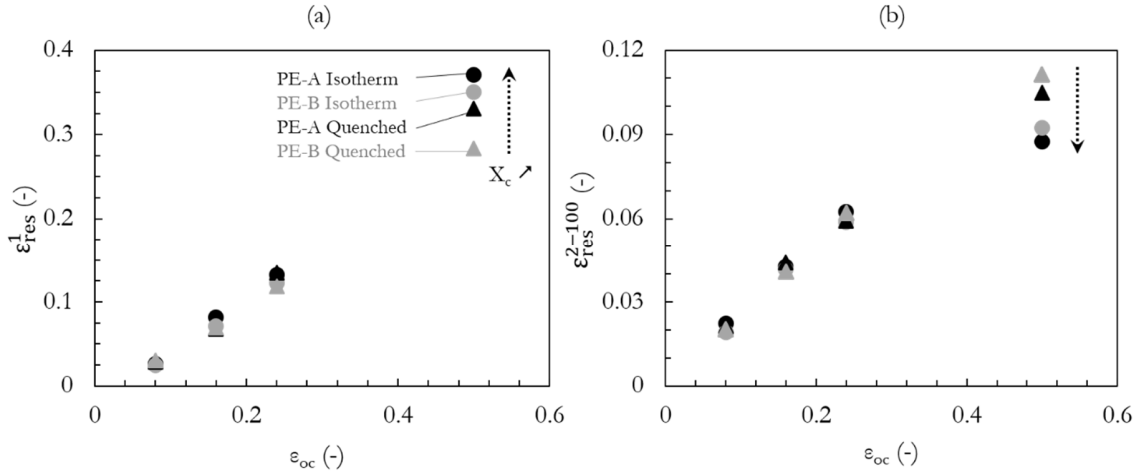

Figure 6: Change of the residual strains as a function of the prescribed maximum strain a) after the 1st cycle, b) from 2nd to 100th cycle

Density of energy dissipated

The hysteresis area W_d^i represents the density of energy dissipated during the i^{th} loading-unloading cycle. The dissipated energy can be ascribed to several mechanisms: for example, the friction between the chains (viscosity), and potential plastic mechanisms such as lamellae fragmentation and/or cavitation[36,37]. The changes of W_d as a function of the cycle number are shown in **Figure 7.** Similar to the residual strain profiles, W_d^1 is much higher than W_d^i (with i >1), confirming major differences between the first and the remaining cycles.

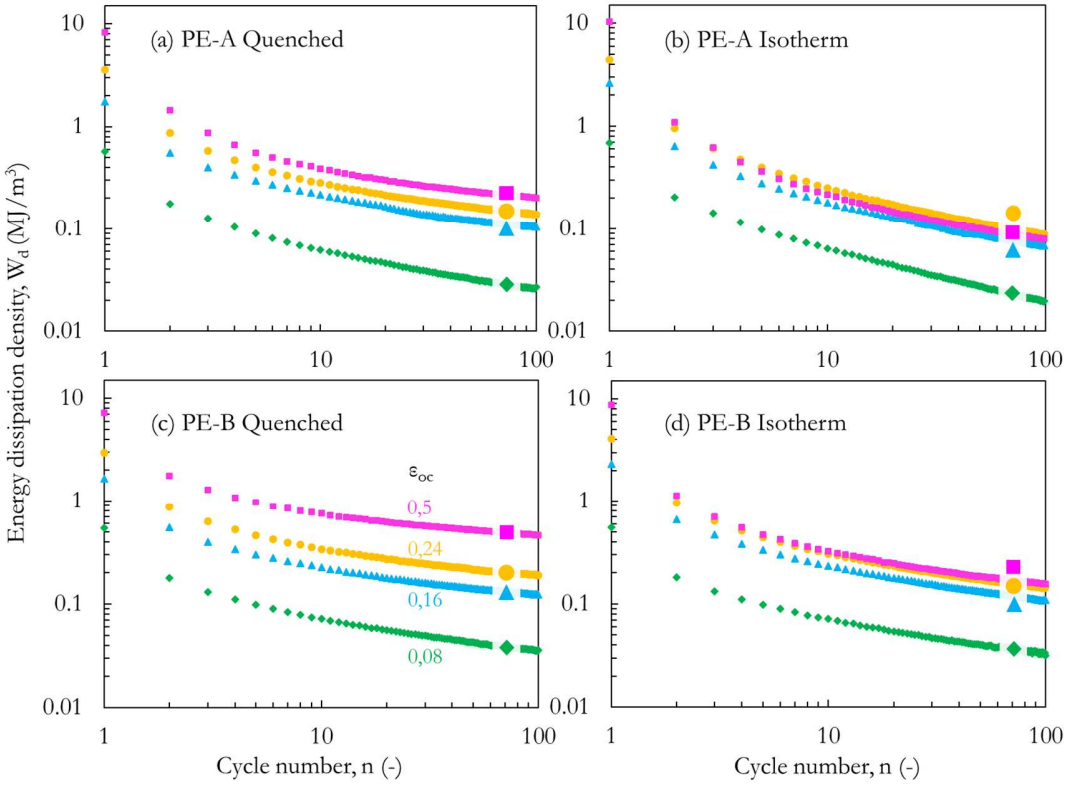

Figure 7: Density of energy dissipation W_d as a function of cycle number in PE samples with different applied oligo-cyclic strains ε_{OC}: (a) PE-A Quenched; (b) PE-A Isothermal; (c) PE-B Quenched and (d) PE-B Isothermal

In **Figure 8a**, for a prescribed ε_{OC}, the isothermal samples tend to dissipate the higher amount of energy per unit volume during the first cycle compared to the quenched ones. The relation between W_d^1 and ε_{OC} is quasi-linear. A simple elastoplastic theory (no hardening) can be used to

approximate and explain their relation, the approximated density of energy dissipation of the first cycle W_d^{1*} is calculated using **equation (7)**.

$$W_d^{1*} = \sigma_{th}(\varepsilon_{OC} - \varepsilon_{th}) \quad (7)$$

Where σ_{th} and ε_{th} are the threshold stress and strain corresponding to the initiation of plasticity (where the stress σ_{th} is set to be 80% of yield stress σ_y obtained by uniaxial tensile curves). The approximated relations are also displayed in **Figure 8a**. Such approximation seems adapted so that the first-cycle induced energy dissipation can be mainly ascribed to the plasticity, it is consistent with the conclusion obtained by residual strain analysis.

The consumed energy per cycle tends to be saturated and approximately identical from the 90th-100th cycle. The energy dissipation during a whole saturated cycle (W_d^{100}) increases as the crystallinity decreases (or ST density increases). This relation is following the aforementioned assumption that the sample deformation remains primarily visco-elastic so that the energy dissipation is mainly caused by the additional viscous effect. W_d^{100}as a function of ε_{OC} of each sample is displayed in **Figure 8b.** The PE-B quenched samples exhibit the highest W_d^{100} value, indicating that this material has a superior energy dissipating capacity in the visco-elastic regime during cyclic deformation due to the more important friction (disentanglement) between the chains.

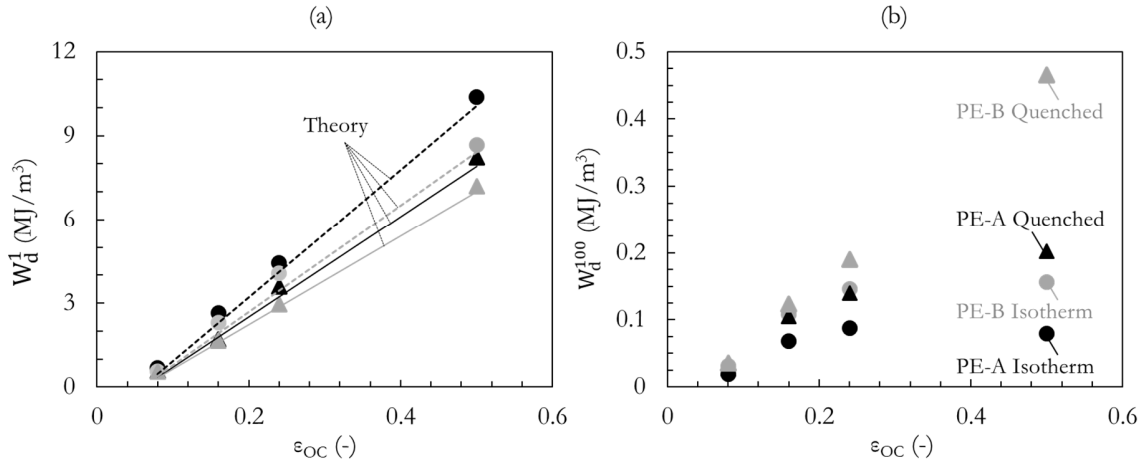

Figure 8: Dissipated energy density of PE samples at different applied oligo-cyclic strains a) after the first loading cycle (W_d^1) and b) after the 100nd loading cycle (W_d^{100})

Change of modulus

As evidenced in **Figure 1**, the experimental stress-strain curves are highly non-linear, therefore, the secant method is widely used to evaluate the modulus at the beginning of each cycle (zero-stress state) [24,26,27,29]. However, to our knowledge, this method has been yet applied to characterize the mixed-mode oligo-cyclic responses of polymers. Indeed, the secant modulus should be measured in the "cycle" with constant stress or strain range, so that the non-linearity effect can be ignored. Yet, by mixed-mode, neither the stress nor the strain amplitude is constant in different cycles. Therefore, an indicator D_E is proposed to evaluate the relative change of the secant modulus is defined as follow. The modulus of each following cycle (2^{nd}-100^{th} cycle) is compared with the modulus of the first cycle respectively. E^{i} and $\mathrm{E}_1^{\mathrm{i}}$ are already defined in the last section **"Description of oligo-cyclic tensile behaviors"**:

$$\mathrm{D}_{\mathrm{E}}^{\mathrm{i}-1} = 1 - \mathrm{E}^{\mathrm{i}} / \mathrm{E}_1^{\mathrm{i}} \qquad (2 \leq i \leq 100) \qquad (8)$$

Although this mechanical indicator D_E is commonly used to evaluate the material damage at macroscale in semi-crystalline polymers[19,24,35], which means that a positive indicator D_E^{i-1} reflecting the decrease of secant modulus is expected. In this work, the negative value is also observed under certain condition and suggest that the modulus of the i^{th} cycle is superior to the initial modulus and indicating a strengthening effect. The changes of D_E in all four PE samples are shown in **Figure 9** as a function of the cycle number. In each sample, it is found that D_E^1 is negative (modulus increases) when ε_{OC} = 0.08 and 0.16. However, D_E^1 becomes positive (modulus decreases) when ε_{OC} = 0.24 and 0.5. From negative to positive, D_E^1 tends to be higher with increasing ε_{OC}. However, during the remaining cycles, D_E values decrease monotonically, indicating the growth of modulus with increasing cycles prior to progressively stabilizing.

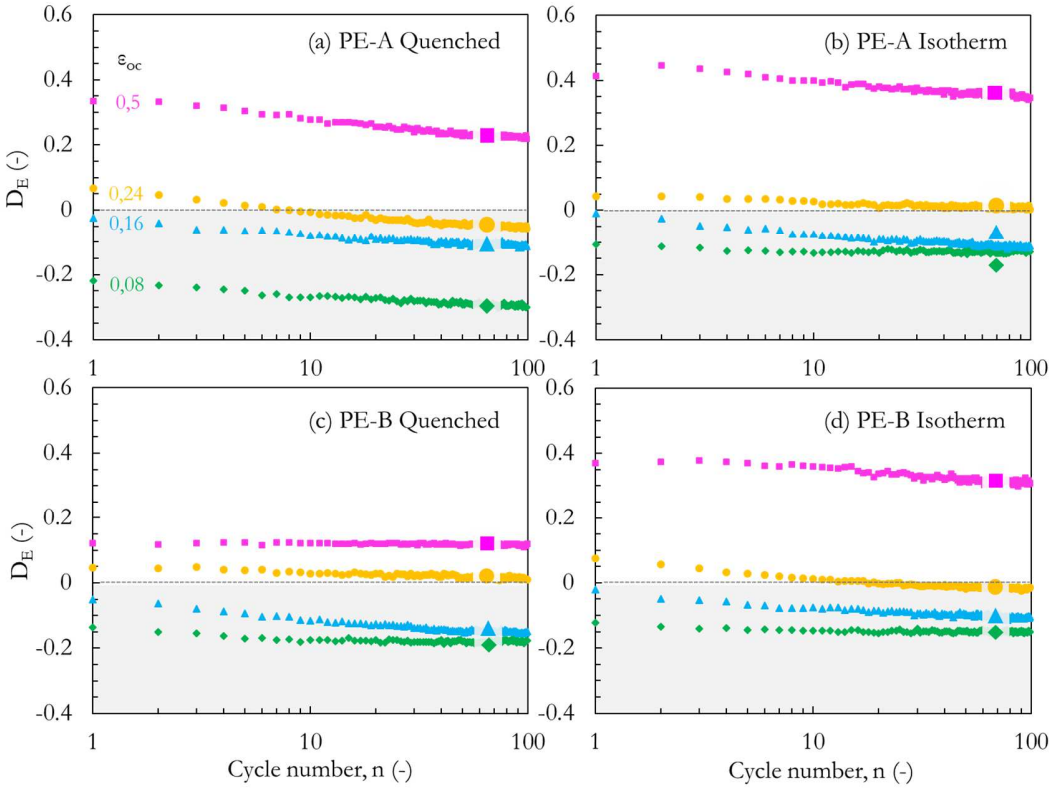

Figure 9: Relative change of the secant modulus evaluated by D_E as a function of cycle number in PE samples with different applied oligo-cyclic strains: (a) PE-A Quenched; (b) PE-A Isothermal; (c) PE-B Quenched and (d) PE-B Isothermal

As mentioned in the introduction, Humbert et *al.* used a model to predict the relation between the elastic modulus and the microstructure of PE [9,12], introducing the use of a mechanical coupling parameter k (the ratio between the stresses concentrated in hard phase and soft phase, σ_h/σ_s), which is physically related to the percolation level of the crystalline phase. The more percolated crystalline structure, the higher k value. The modulus is estimated using relation (9) where φ_h is the volume fraction of hard phase and E_s is the modulus of the soft phase.

$$E \approx k\mathrm{E_s} \times \frac{\varphi_\mathrm{h}}{1-\varphi_\mathrm{h}} \tag{9}$$

Neglecting the influence of the interphase, the hard and soft phases are simply considered as the crystalline and amorphous phases[12]. Within this theoretical framework, three microstructural parameters (k, E_s, and φ_h) can directly determine the macroscopic modulus. Therefore, the modulus change can be related to different mechanisms that modify these parameters.

Firstly, the plastic deformation can provoke the decrease of E_s and k due to the disentanglement/rupture of weak chains (they may also induce cavitation) and fragmentation of the percolated crystalline structure respectively. However, to interpret the initial negative values of D_E (the first-cycle induced increase of modulus) under certain loading conditions (ε_{OC} = 0.08 and 0.16) and the decrease of D_E in the subsequent cycles (rest-cycles induced increase of modulus), the aforementioned competing mechanism should be mentioned again. As it compensates the stress softening, the orientation/alignment of chains and the stretching of stress transmitters can result in partial recrystallization, potentially increasing both the fraction of hard phase φ_h, amorphous modulus E_s. Also, the recrystallization may bridge the fragmented crystalline network and increase the k value.

Regarding D_E^1, with increasing ε_{OC}, the effect of "structural deteriorations" on the modulus becomes more and more dominant compared to the recrystallization at the zero-stress state. However, differing from the first cycle, the chain orientation/recrystallization governs the modulus of the consecutive cycles.

Figure 10 shows that the values of D_E^1 in all four samples increase as a function of ε_{OC}. For the relatively lower ε_{OC} (0.08/0.16/0.24), the dependency of D_E^1 on the microstructural properties remains unclear. However, when ε_{OC} = 0.5, D_E^1 value becomes higher as the sample crystallinity increases or ST density decreases. Indeed, the sample with higher crystallinity should have a more percolated crystalline structure, when the imposed strain is high enough, the crystalline network is nearly all broken, so it shows a more important loss of percolation, k decreases from a very high value to almost 1[12]. Additionally, the lower ST density promotes the disentanglement and chain rupture that could also induce a more important loss of amorphous modulus.

Physically, it seems reasonable that under a given loading condition, the recrystallization at zero-stress state should be more effective in the quenched samples during the following cycles due to their larger number of STs and higher residual strain in the amorphous phase (the chains are more stretched). However, the relation between the following-cycles-induced strengthening effect (decrease of D_E as a function of cycle number) and pristine PE microstructure is not clear. It may be interpreted as the complicated relations between the orientation of chains/recrystallization and the relative evolutions of the three parameters (k, E_s, and φ_h).

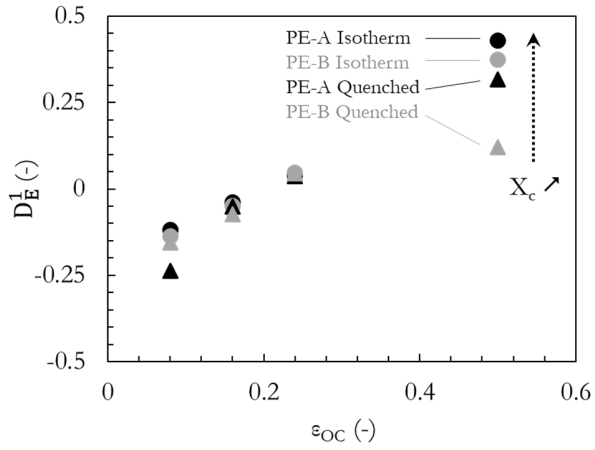

Figure 10: D_E^1 of PE samples at different applied oligo-cyclic strains ε_{OC}

Physical scenario

According to all the aforementioned changes of the mechanical indicators, and the microscopic interpretations, a physical scenario describing the microstructural deformation mechanisms is proposed. The schematic is shown in **Figure 11.** It worth noting that the cavitation is not mentioned here, indeed, the origin of this phenomenon is related to the disentanglement/rupture of chains[35,41].

The pristine HDPE microstructure is composed of spherulites with radially oriented crystalline lamellae within the amorphous matrix. Several lamellae are percolated. Considering the ε_{OC} range under investigation, STs have different resistance against the deformation. The "strong" tie molecules can continually act without rupture, whereas the "weak" entanglement or loops, can be unfolded due to the slip of chains.

During the first loading, the very weak active entanglement/loops slip and unfold even at low macroscopic strain, followed by the elimination of percolation and shearing of crystals when the imposed strain reaches the plastic regime. The higher imposed strain, the more complete breakage of the crystalline network and disentanglement. In particular, the elimination of crystalline percolation tends to activate the confined STs that do not transmit the stress during the first cycle due to the percolated crystalline structure. The tie molecules with high deformation capacity can be aligned and may lead to the recrystallization, which can partially disappear during the unloading. Comparing the pristine (undeformed) state and the 1st zero-stress

state, the orientation of chains/recrystallization competes with the structural deteriorations (disentanglement/rupture of STs and breakage of the crystalline network): in the low strain range (ε_{OC} = 0.08 and 0.16), the recrystallization dominates and results in a higher apparent modulus whereas in the high strain range (ε_{OC} = 0.24 and 0.5), the structural deteriorations prevail, the modulus after the first cycle is inferior to the initial one.

During the following cycles, the main deformation is ascribed to the amorphous phase. At the maximum-strain state, the level of chain orientation/recrystallization does not change with increasing cycles due to the constant imposed strain (ε_{OC}), therefore, the progressive stress softening is governed by the disentanglement occurring in the pre-confined regions and successive breakage of the crystalline network (if it is not completely broken by the first loading). With increasing ε_{OC}, the first cycle can induce more important structural deteriorations, which means that fewer STs that can be potentially disentangled, and less crystalline percolation remains after the first cycle. Regarding the zero-stress state, due to the accumulation of residual strain, the effect of recrystallization increases crucially as a function of cycle number. And the successive structural deteriorations cannot counteract this effect on modulus, the modulus thus tends to be a higher value with increasing cycles.

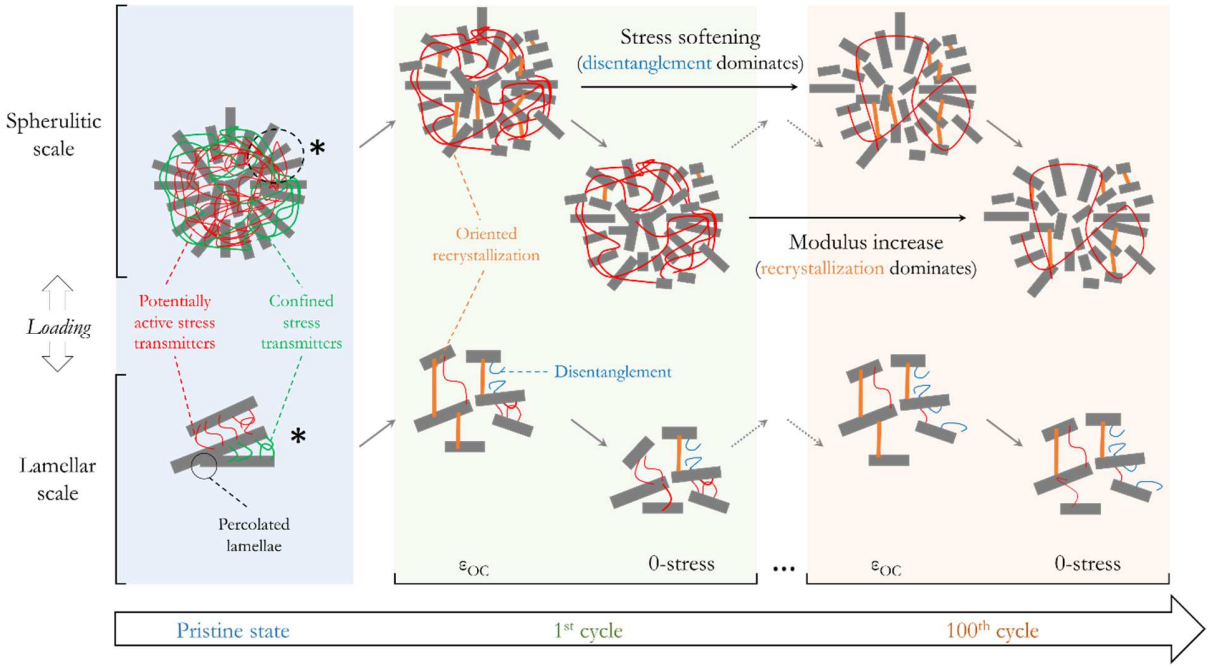

Figure 11: The physical scenario of HDPE under mixed-mode oligo-cyclic loading conditions (spherulitic scale and lamellar scale)

Post-cyclic tensile behavior

Uniaxial tension until failure was achieved after a series of 10 cycles as most of the microstructure changes were proven to occur within this period. All the PE samples show the *Mullins-like* behavior, as an example, the post-cyclic tensile behaviors of the PE-A isothermal sample are superimposed in **Figure 12a**: the post-cyclic curves tend to match the pristine one for strain larger than the ones endured during the oligo-cyclic test ($\varepsilon > \varepsilon_{OC}$), suggesting that all the changes occurring in the following cycles (2^{nd}-100^{th}) have a limited influence on the overall short-term mechanical performance. However, regarding fracture performance, the remaining toughness, W_f was then estimated as indicated in **Figure 12b**, where the multi-step stress-strain profile of PE-A isothermal sample with ε_{OC} = 0.5 is displayed as an example. Within this method, the first-cycle-induced damage (related to the loss of tensile toughness) is also taken into account. **Figure 12c** gives the relation between W_f and ε_{OC}. W_f for ε_{OC} = 0 naturally corresponds to the tensile toughness of the pristine PE samples, and the error bar indicates the difference between the maximum/minimum values. For a given grade (PE-A or PE-B), the value W_f does not significantly differ by the heat treatments, the isothermal samples require just slightly more energy until fracture (10% for PE-B and 8% for PE-A). However, between PE-A and PE-B samples, the difference is important (about 30%), which means that pristine W_f shows a more crucial dependency on the molecular characteristics than thermal treatment. Also, it is found that the W_f values of all four samples remain almost constant indicating that the change of energy required to failure is not measurable when ε_{OC} does not exceed 0.24. However, when ε_{OC} = 0.5, in the PE-A isothermal sample, which has the lowest ST density and highest crystallinity, the W_f decreases about 25%. This result tends to confirm that the resistance to failure decreases so that the mechanical damage should be relatively more important in PE-A isothermal sample than others.

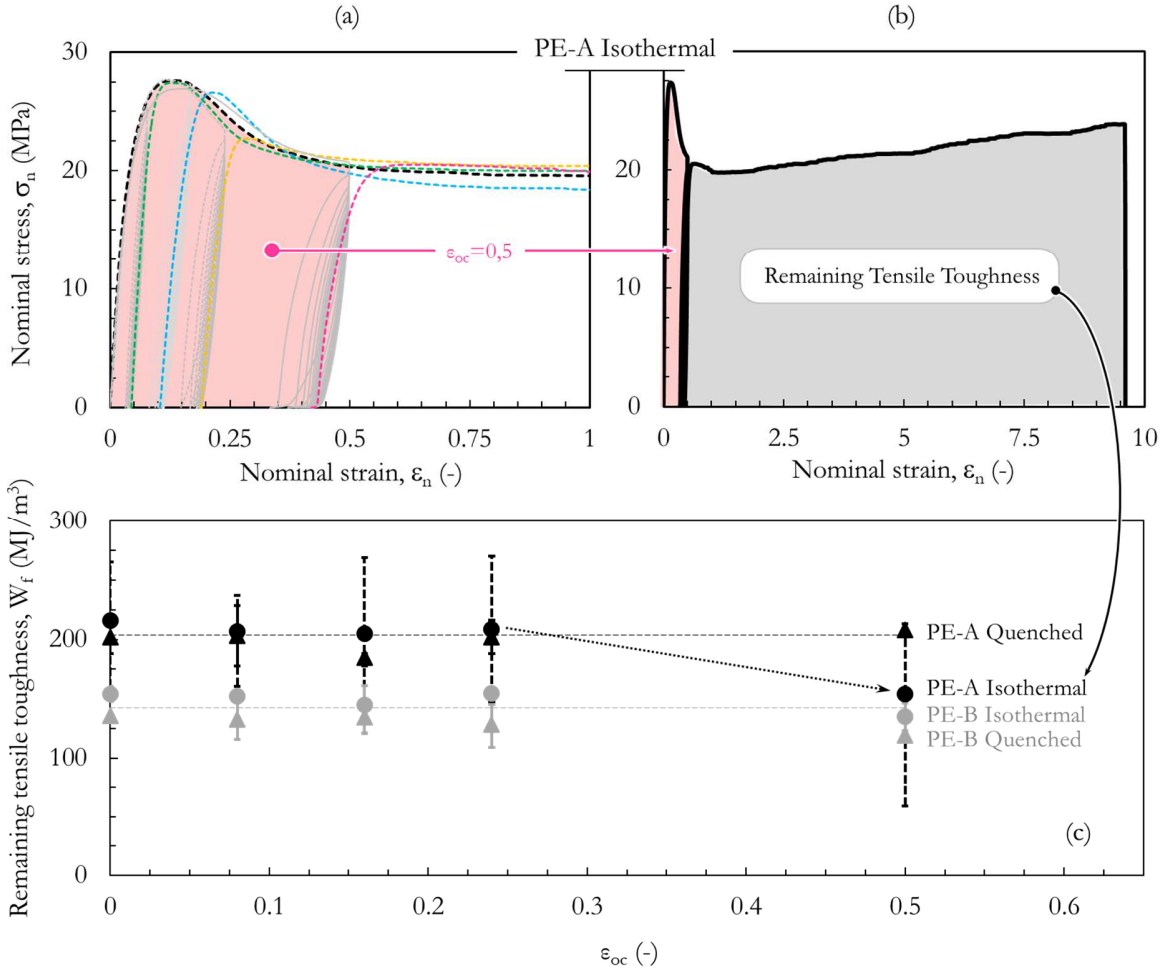

Figure 12: a) Mullins-like behavior of PE-A isothermal sample; b) Definition of remaining tensile toughness (ex. PE A isothermal sample, with ε_{OC}=0.5), c) Remaining tensile toughness in different samples as function ε_{OC}

CONCLUSION

The performance of varying HDPE samples under oligo-cyclic loading conditions was evaluated and a physical scenario is proposed for the interpretation of the measured macro-micro correlations: the structural deteriorations, such as chain rupture/disentanglement and breakage of lamellae/percolation are mainly induced by the first cycle. These structural deteriorations can induce the loss of modulus and compete with the orientation of stress transmitters/recrystallization associated with the strengthening effect. When the imposed cyclic

strain is high enough (ε_{OC}=0.5), during the following cycles, the structural deteriorations are mainly assigned to the pre-confined disentanglement in the amorphous phase, dominating the stress change (decrease) at maximum strain state. However, at the zero-stress state, the chain orientation/recrystallization plays a more crucial role as illustrated by the increase of apparent modulus. Noticeably, the mechanical losses during the cyclic deformation including the stress softening and the decrease of the apparent modulus are more crucial in the isothermal samples, especially the PE-A grade, having higher crystallinity and lower ST density. However, it seems that the microstructural/mechanical changes during the following cycles have a limited effect on the further tensile loading path. However, for the tensile toughness, considering the effect of the complete loading process including the first cycle, there is a loss in the PE-A isothermal sample with the "extreme" microstructural parameters.

Compared to the other HDPE, the one for PE-100 pipeline (PE-B in this study) has relatively lower yield stress, modulus and tensile toughness. However, this material shows a better resistance against the mechanical losses under oligo-cyclic loading conditions. Even when ε_{OC} = 0.5, neither the quenched nor the isothermal sample is significantly damaged after the tests. Moreover, the more important energy dissipation at the end of oligo-cyclic tests is observed in PE-B samples especially the quenched one. It means that PE-B also has a more performant capacity to continually dissipate the seismic energy, due to the limited damage, it means that this material is more performable to consume the energy and protect the whole architecture.

ACKNOWLEDGEMENTS

The authors are indebted to INEOS (Brussels, Belgium) for supplying the HDPE polymers and their molecular characteristics. The SWING beamline in French SOLEIL synchrotron is appreciated for time allocation. *EDF-DIPNN Direction Technique* and *EDF lab R&D Les Renardières* are acknowledged for the grant of a doctoral fellowship to H. GUO.

Reference

[1] N. Nishonov, D. Bekmirzaev, E. An, Z. Urazmukhamedova, K. Turajonov, Behaviour and Calculation of Polymer Pipelines Under Real Earthquake Records, in: IOP Conf. Ser. Mater. Sci. Eng., IOP Publishing, 2020: p. 052076.

[2] Hideki Omuro, Tomokazu Himono, POLYETHYLENE PIPELINE PERFORMANCE AGAINST EARTHQUAKE, in: 2018.
[3] Angelo Masi, Giuseppe Santarsiero, Domenico Nigro, Cyclic tests on external RC beam-column joints: role of seismic design level and axial load value on the ultimate capacity, J. Earthq. Eng. 17 (2013) 110–136.
[4] Paolino Cassese, Paolo Ricci, Gerardo M. Verderame, Experimental study on the seismic performance of existing reinforced concrete bridge piers with hollow rectangular section, Eng. Struct. 144 (2017) 88–106.
[5] B. Xiong, O. Lame, J. M. Chenal, C. Rochas, Roland Seguela, G. Vigier, In-situ SAXS study and modeling of the cavitation/crystal-shear competition in semi-crystalline polymers: Influence of temperature and microstructure in polyethylene, Polymer. 54 (2013) 5408–5418.
[6] Bijin Xiong, Olivier Lame, Jean-Marc Chenal, Cyrille Rochas, Roland Seguela, Gerard Vigier, In-situ SAXS study of the mesoscale deformation of polyethylene in the pre-yield strain domain: Influence of microstructure and temperature, Polymer. 55 (2014) 1223–1227.
[7] B. Xiong, O. Lame, J. M. Chenal, C. Rochas, Roland Seguela, On the strain-induced fibrillar microstructure of polyethylene: Influence of chemical structure, initial morphology and draw temperature, Express Polym. Lett. 10 (2016) 311.
[8] R. Séguéla, On the Natural Draw Ratio of Semi-Crystalline Polymers: Review of the Mechanical, Physical and Molecular Aspects, Macromol. Mater. Eng. 292 (2007) 235–244.
[9] S. Humbert, O. Lame, R. Séguéla, G. Vigier, A re-examination of the elastic modulus dependence on crystallinity in semi-crystalline polymers, Polymer. 52 (2011) 4899–4909.
[10] Bijin Xiong, Olivier Lame, Jean-Marc Chenal, Yongfeng Men, Roland Seguela, Gerard Vigier, Critical stress and thermal activation of crystal plasticity in polyethylene: Influence of crystal microstructure and chain topology, Polymer. 118 (2017) 192–200.
[11] S. Humbert, O. Lame, G. Vigier, Polyethylene yielding behaviour: What is behind the correlation between yield stress and crystallinity?, Polymer. 50 (2009) 3755–3761.
[12] T. Deplancke, M. Fivel, O. Lame, 1D strain rate-dependent constitutive model of UHMWPE: From crystalline network to fibrillar structure behavior, Mech. Mater. 137 (2019) 103129.
[13] B. Xiong, O. Lame, J.-M. Chenal, C. Rochas, R. Seguela, G. Vigier, Amorphous phase modulus and micro–macro scale relationship in polyethylene via in situ SAXS and WAXS, Macromolecules. 48 (2015) 2149–2160.
[14] Y.-Q. Zhou, N. Brown, The mechanism of fatigue failure in a polyethylene copolymer, J. Polym. Sci. Part B Polym. Phys. 30 (1992) 477–487.
[15] J. Runt, M. Jacq, Effect of crystalline morphology on fatigue crack propagation in polyethylene, J. Mater. Sci. 24 (1989) 1421–1428.
[16] J.T. Yeh, J. Runt, Fatigue crack propagation in high-density polyethylene, J. Polym. Sci. Part B Polym. Phys. 29 (1991) 371–388.
[17] M. Niinomi, L. Wang, T. Enjitsu, K.-I. Fukunaga, Fatigue characteristics of ultra high molecular weight polyethylene with different molecular weight for implant material, J. Mater. Sci. Mater. Med. 12 (2001) 267–272.
[18] N. Brown, X. Lu, Y.-L. Huang, R. Qian, Slow crack growth in polyethylene-a review, in: Makromol. Chem. Macromol. Symp., Wiley Online Library, 1991: pp. 55–67.

[19] Y. Zhang, P.-Y.B. Jar, S. Xue, L. Li, Quantification of strain-induced damage in semi-crystalline polymers: a review, J. Mater. Sci. 54 (2019) 62–82.
[20] Sandrine Humbert, O. Lame, J. M. Chenal, C. Rochas, G. Vigier, New insight on initiation of cavitation in semicrystalline polymers: in-situ SAXS measurements, Macromolecules. 43 (2010) 7212–7221.
[21] W. Liu, Z. Gao, Z. Yue, Steady ratcheting strains accumulation in varying temperature fatigue tests of PMMA, Mater. Sci. Eng. A. 492 (2008) 102–109.
[22] G. Tao, Z. Xia, Fatigue behavior of an epoxy polymer subjected to cyclic shear loading, Mater. Sci. Eng. A. 486 (2008) 38–44.
[23] G. Kang, Y. Liu, Y. Wang, Z. Chen, W. Xu, Uniaxial ratchetting of polymer and polymer matrix composites: time-dependent experimental observations, Mater. Sci. Eng. A. 523 (2009) 13–20.
[24] Elodie Mourglia-Seignobos, Didier R. Long, Ludovic Odoni, Loïc Vanel, Paul Sotta, Cyrille Rochas, Physical mechanisms of fatigue in neat polyamide 6, 6, Macromolecules. 47 (2014) 3880–3894.
[25] A.D. Drozdov, Cyclic viscoelastoplasticity and low-cycle fatigue of polymer composites, Int. J. Solids Struct. 48 (2011) 2026–2040.
[26] N. Fouchier, C. Nadot-Martin, E. Conrado, A. Bernasconi, S. Castagnet, Fatigue life assessment of a Short Fibre Reinforced Thermoplastic at high temperature using a Through Process Modelling in a viscoelastic framework, Int. J. Fatigue. 124 (2019) 236–244.
[27] B. Klimkeit, S. Castagnet, Y. Nadot, A. El Habib, G. Benoit, S. Bergamo, C. Dumas, S. Achard, Fatigue damage mechanisms in short fiber reinforced PBT+ PET GF30, Mater. Sci. Eng. A. 528 (2011) 1577–1588.
[28] A. Avanzini, Mechanical characterization and finite element modelling of cyclic stress–strain behaviour of ultra high molecular weight polyethylene, Mater. Des. 29 (2008) 330–343.
[29] A.D. Drozdov, Cyclic strengthening of polypropylene under strain-controlled loading, Mater. Sci. Eng. A. 528 (2011) 8781–8789.
[30] A.D. Drozdov, J. deC Christiansen, Cyclic viscoplasticity of high-density polyethylene: experiments and modeling, Comput. Mater. Sci. 39 (2007) 465–480.
[31] A. D. Drozdov, Mullins' effect in semicrystalline polymers, Int. J. Solids Struct. 46 (2009) 3336–3345.
[32] M. Makki, G. Ayoub, H. Abdul-Hameed, F. Zaïri, B. Mansoor, M. Naït-Abdelaziz, M. Ouederni, Mullins effect in polyethylene and its dependency on crystal content: a network alteration model, J. Mech. Behav. Biomed. Mater. 75 (2017) 442–454.
[33] R.W. Meyer, L.A. Pruitt, The effect of cyclic true strain on the morphology, structure, and relaxation behavior of ultra high molecular weight polyethylene, Polymer. 42 (2001) 5293–5306.
[34] F. Xu, N. Aravas, P. Sofronis, Constitutive modeling of solid propellant materials with evolving microstructural damage, J. Mech. Phys. Solids. 56 (2008) 2050–2073.
[35] F. Detrez, S. Cantournet, R. Seguela, Plasticity/damage coupling in semi-crystalline polymers prior to yielding: Micromechanisms and damage law identification, Polymer. 52 (2011) 1998–2008.
[36] Z. Qi, N. Hu, D. Zeng, X. Su, Failure of high density polyethylene under cyclic loading: Mechanism analysis and mode prediction, Int. J. Mech. Sci. 156 (2019) 46–58.

[37] R.P. Janssen, D. de Kanter, L.E. Govaert, H.E. Meijer, Fatigue life predictions for glassy polymers: a constitutive approach, Macromolecules. 41 (2008) 2520–2530.
[38] L. Mullins, Permanent set in vulcanized rubber, Rubber Chem. Technol. 22 (1949) 1036–1044.
[39] Leonard Mullins, Softening of rubber by deformation, Rubber Chem. Technol. 42 (1969) 339–362.
[40] Julie Diani, Bruno Fayolle, Pierre Gilormini, A review on the Mullins effect, Eur. Polym. J. 45 (2009) 601–612.
[41] F.P.C. Gomes, M.R. Thompson, Analysis of Mullins effect in polyethylene using ultrasonic guided waves, Polym. Test. 60 (2017) 351–356.
[42] G. Ayoub, F. Zaïri, M. Naït-Abdelaziz, J.M. Gloaguen, Modeling the low-cycle fatigue behavior of visco-hyperelastic elastomeric materials using a new network alteration theory: application to styrene-butadiene rubber, J. Mech. Phys. Solids. 59 (2011) 473–495.
[43] S. Humbert, O. Lame, J.-M. Chenal, R. Seguela, G. Vigier, Memory effect of the molecular topology of lamellar polyethylene on the strain-induced fibrillar structure, Eur. Polym. J. 48 (2012) 1093–1100.
[44] Z. Jiang, Y. Tang, J. Rieger, H.-F. Enderle, D. Lilge, S.V. Roth, R. Gehrke, W. Heckmann, Y. Men, Two lamellar to fibrillar transitions in the tensile deformation of high-density polyethylene, Macromolecules. 43 (2010) 4727–4732.
[45] A. Alizadeh, L. Richardson, J. Xu, S. McCartney, H. Marand, Y. W. Cheung, S. Chum, Influence of structural and topological constraints on the crystallization and melting behavior of polymers. 1. Ethylene/1-octene copolymers, Macromolecules. 32 (1999) 6221–6235.
[46] S. Humbert, O. Lame, G. Vigier, Influence de la topologie moléculaire et de la microstructure sur les propriétés mécaniques des Polyéthylènes, Lab. Rech. MATEIS INSA Lyon. (2009).
[47] L. Hubert, L. David, R. Seguela, G. Vigier, C. Degoulet, Y. Germain, Physical and mechanical properties of polyethylene for pipes in relation to molecular architecture. I. Microstructure and crystallisation kinetics, Polymer. 42 (2001) 8425–8434.
[48] B. Crist, C.J. Fisher, P.R. Howard, Mechanical properties of model polyethylenes: tensile elastic modulus and yield stress, Macromolecules. 22 (1989) 1709–1718.
[49] Y.-L. Huang, N. Brown, The effect of molecular weight on slow crack growth in linear polyethylene homopolymers, J. Mater. Sci. 23 (1988) 3648–3655.
[50] Y.-L. Huang, N. Brown, Dependence of slow crack growth in polyethylene on butyl branch density: morphology and theory, J. Polym. Sci. Part B Polym. Phys. 29 (1991) 129–137.
[51] Séverine Humbert, Olivier Lame, Jean-Marc Chenal, Cyrille Rochas, Gérard Vigier, Small strain behavior of polyethylene: in situ SAXS measurements, J. Polym. Sci. Part B Polym. Phys. 48 (2010) 1535–1542.
[52] V. Gaucher–Miri, C. Depecker, R. Séguéla, Reversible strain-induced order in the amorphous phase of a low-density ethylene/butene copolymer, J. Polym. Sci. Part B Polym. Phys. 35 (1997) 2151–2159.
[53] W.W. Adams, D. Yang, E.L. Thomas, Direct visualization of microstructural deformation processes in polyethylene, J. Mater. Sci. 21 (1986) 2239–2253.